Reverse time migration from rugged topography to image ground-penetrating radar data in complex environments

John H Bradford*, Janna Rozar, David Wilkins
Department of Geosciences, Boise State University

Richard Ford
Department of Geosciences, Weber State University

***Abstract*—In GPR imaging, it is common for the depth of investigation to be on the same order as the variability in surface topography. In such cases, migration fails when it is carried out from a datum after application of elevation statics. We introduce a reverse-time migration algorithm where the wavefield extrapolation is computed directly from the acquisition surface without the need for datuming. In a synthetic and field example the algorithm shows significant improvement over a processing sequence where migration is performed after elevation statics.**

Keywords—reverse time migration; GRP; RTM; complex environments

I. INTRODUCTION

Although computationally expensive, hardware advances over the past two decades have made reverse-time depth migration (RTM) feasible for many applications in shallow seismic and GPR imaging. RTM is routinely applied to large exploration seismic datasets and is the preferred imaging tool. The advantage of RTM implemented with the full wave-equation is that it honors the physics of wave propagation more closely than other migration methods and therefore can produce the most accurate images. RTM is not limited by reflector dip or velocity heterogeneity. RTM is attractive for true amplitude imaging as it inherently accounts for wavefront spreading. Additionally, attenuation and transmission losses can be incorporated into the RTM framework[1]. Here we focus on RTM in the post-stack domain.

Several authors have applied reverse time migration algorithms to GPR data. Fisher et al. (1992) gave perhaps the first example, where they utilized an acoustic algorithm and the exploding reflector model for post-stack migration of GPR data[2]. Sanada and Ashida (1999) developed an RTM post-stack algorithm from Maxwell's equations that includes the effect of conductivity.As described by Lehmann and Green (2000), topographic variation on the same order as depth of investigation can have serious consequences on kinematic reconstruction of GPR images when conventional processing strategies are applied, e.g. elevation statics followed by post-stack[3,4] migration (Fig.1); an alternative processing

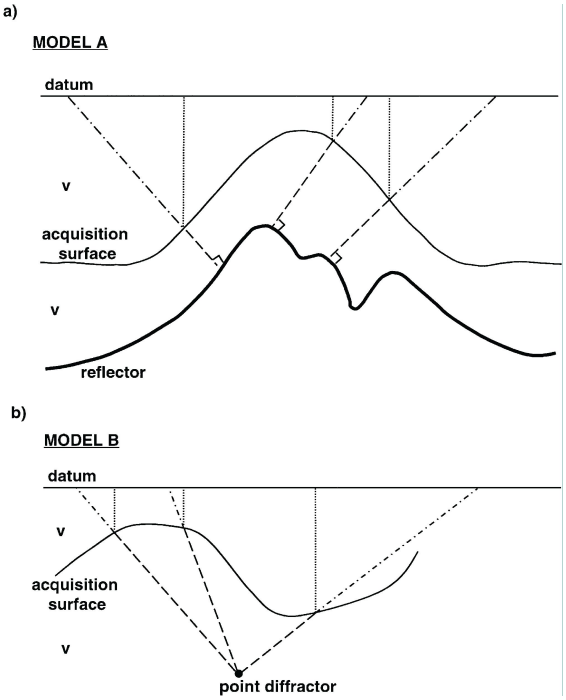

Fig.1 Schematic of travel paths for a zero offset section, collected along a topographic surface, after correction to a datum. The vertical dashed lines show the travel path which is implicitly assumed in a standard elevation static correction. The dashed dot line shows the correct travel path. The assumed path is a poor approximation leading to failure of migration from datum after elevation statics corrections. (Source: Lehmann and Green, 2000)

strategy must be employed under these conditions. We have extended the RTM post-stack approach for imaging in complex topography based on the exploding reflector concept. The downward wavefield extrapolation is implemented directly from the topographic surface thereby avoiding the need for elevation statics or datuming. Additionally, the algorithm is based on the wave equation solution of Maxwell's equations and can account for complex velocity and conductivity distributions.

II. The RTM Algorithm

RTM is conceptually simple: The recorded wavefield is extrapolated into the subsurface by solving Maxwell's equations with a negative time step and inserting the radargram as a boundary condition at the surface in reverse time order. In the poststack case, the imaging condition is met when clock has counted backward to zero time - ie. all the recorded energy has been injected back into the model and propagated downward to its point of origin. We utilize the decoupled, second order differential form of Maxwell's equations. In 2D, with the electric field polarized perpendicular to the image plane (TE mode), this reduces to the damped scalar wave equation:

$$\mu\varepsilon'\frac{\partial^2 E}{\partial t^2}+\mu\sigma'\frac{\partial E}{\partial t}=\frac{\partial^2 E}{\partial x^2}+\frac{\partial^2 E}{\partial y^2} \qquad (1)$$

Where E is the electric field, μ is the magnetic permeability, t is time, and x and z are the spatial variables. The primed variables ε' and σ' are the apparent dielectric permittivity and electric conductivity. In the exploding reflector model, the field is approximated with one-way propagation and the model velocity is one half of the true velocity. This change of variables requires that ε' =4ε in equation 1 where ε is the true permittivity. Additionally we include attenuation in our formulation, and assume that the low loss approximation holds, implying that $\alpha'=\frac{\sigma'}{2}\sqrt{\frac{\mu}{\varepsilon'}}$. In this case, it is easy to show that and σ' =4σ, where σ is the true electric conductivity of the medium. We assume that μ is equal to the permeability of free space. We solve the wave equation using a 2nd order accurate finite difference algorithm with perfectly matched layer (PML) absorbing boundary conditions as formulated for the scalar wave equation by Zhou et al. (2001) which leads to sets of coupled anisotropic equations to solve in the boundary region.

The algorithm is implemented in Matlab with computational efficiency gained by using matrix calculations to take advantage of multi-core/processor systems. The wavefield extrapolation is computed using a negative time step. The recorded wavefield is input as a boundary condition in reverse time order along the recording or topographic surface. Since the algorithm is computed on a square grid, some error is introduced by the grid discontinuities along the surface. Because these discontinuities are much smaller than a wavelength the introduced errors are minimal (~1/10 λ at the highest frequency in the data).

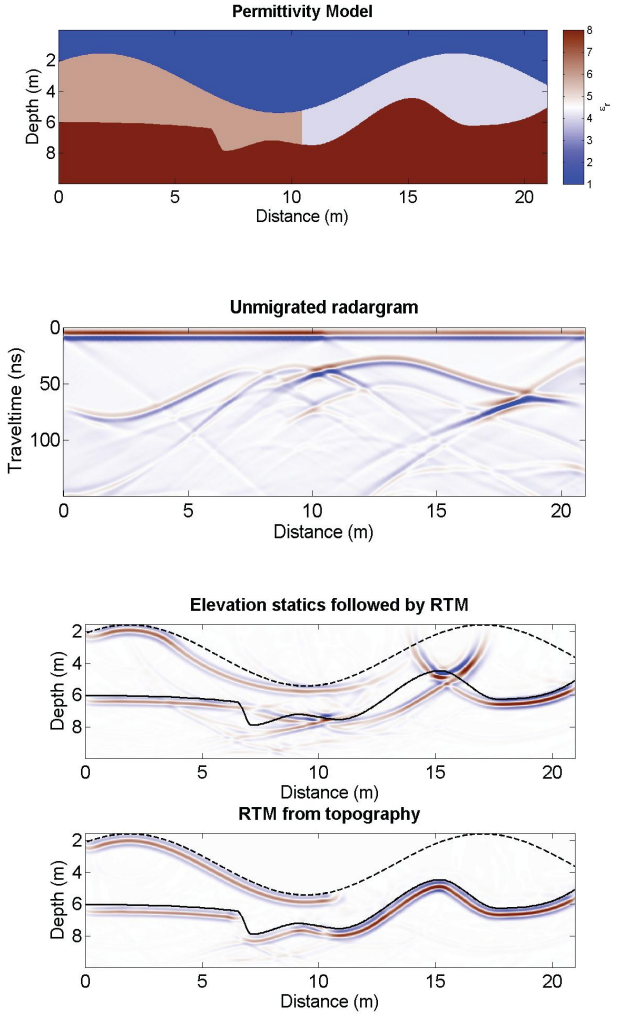

Fig.2 A major benefit of RTM is its ability to handle large lateral velocity contrasts. In this case the left half of the model contains low velocity material. Migration fails in this case when applied after elevation statics. RTM from topography accurately reconstructs the image even with abrupt lateral gradients and avoids the need for datuming.

III. Synthetic Example

A major benefit of RTM is its ability to handle large lateral velocity contrasts. To test both the response of our algorithm to abrupt lateral velocity changes and severe topography relative to the depth of investigation, we construct the model shown in

Fig.2. The sinusoidal surface topography has a trough to peak height of 4 m and the depth to the irregular reflecting layer varies from 1-5 m. The low permittivity upper layer has an abrupt decrease in permittivity halfway across the model. We tested two processing schemes: 1) conventional flow with elevation statics followed by RTM, and 2) RTM from topography. For elevation statics, the replacement velocity was the higher velocity material.

RTM from datum after elevation statics was carried out with the correct velocity model, yet the image is poorly focused and reflections are not correctly located (Fig.2). Note the syncline centered at a distance of 15 m along the profile. It appears to be over-migrated which could lead to the erroneous conclusion that the velocity model is incorrect (Fig.2). RTM from topography accurately reconstructs the image producing a sharp image of the reflecting boundary even in the area of the vertical velocity contrast in the overburden (Fig.2).

IV. Field Test: Coral Pink Sand Dunes, Utah, USA

The Coral Pink Sand Dunes (CPSD) is located in southern Utah and is one of the largest dune - fields in the Great Basin–Colorado Plateau Transition Zone. The CPSD rests on Navajo Sandstone, and is bisected by the Sevier Normal Fault, which also forms the bedrock escarpment along the eastern boundary of the lower dune field (LDF). To test the hypothesis that fault controlled topography along the underlying bedrock surface controls dune formation and geometry, we carried out a ground-penetrating radar (GPR) study. Our primary objective was to map the dune bedrock interface and to image structural features within the bedrock. We collected over 20 km of profiles along 25 transects with 50 and 100 MHz antennas. Elevation control was maintained using continuous GPS with differential corrections made in post-processing. The GPS base station was located within 10 km of all transects. The GPS and GPR positions were linked by syncing the GPR acquisition clock to the GPS clock. GPR signal penetration was excellent and we recorded reflections at depths of greater than 35 m in some locations. This provided excellent images of both the modern dunes and the underlying ancient dune stratigraphy. Outcrops and/or shallow boreholes along some transects provide ground truth for dune-bedrock contacts. While GPR signal quality was excellent, topographic and stratigraphic complexity provided an imaging challenge at the site. Surface topography varied by more than 25 m along some profiles with sustained gradients of greater than 30 degrees.

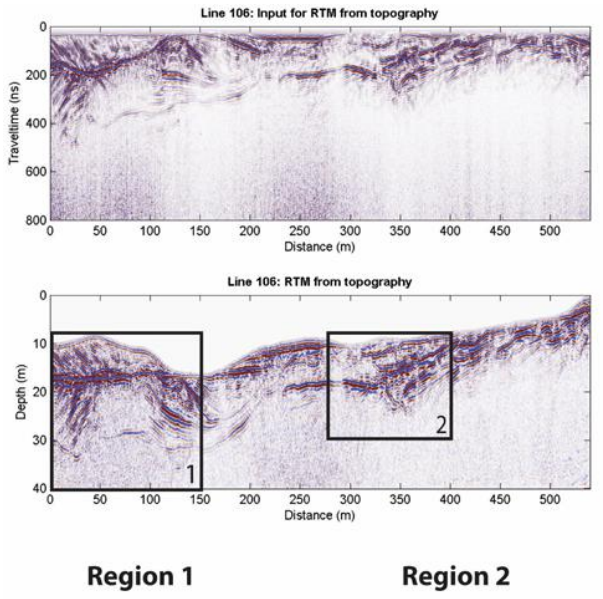

Fig.3 An example profile from the CPSD survey showing the preprocessed data prior to migration and the data after RTM. In Regions 1 and 2 we compare RTM after elevation statics to RTM from topography. In Region 1, note the incorrect placement of steeply reflections within the bedrock stratigraphy from 20-30 m depth at distances of less than 50 m and poor focusing between 100 and 125 m distance when migrated from datum. In Region 2 there is an event dipping steeply to the right between 340 and 360 m that we interpret as a normal fault. The fault plane is well focused with RTM from topography but difficult to interpret when migrated from datum.

Fig.3 illustrates a typical profile with some particularly interesting features. In general, we see the modern dune sand lying on top of the bedrock surface, with bedrock comprised of ancient lithified dunes. Bedrock is often exposed in the intradune areas. Region 1 is a zone of steeply dipping bedforms within the bedrock stratigraphy and Region 2 contains a feature we have interpreted as a normal fault within the bedrock. In both cases, the image is substantially improved by RTM from topography.

V. Conclusion

When imaging complex stratigraphy beneath rugged topography the kinematics of the recorded wavefield deviate significantly from the assumption of vertical near surface propagation that is implicit in standard elevation static corrections. Migration from datum after such corrections significantly distorts the image leading to poor focusing and incorrect positioning of reflections. RTM from topography correctly treats the wavefield kinematics and produces an accurate image, even in the presence of large lateral velocity gradients. Precise horizontal and vertical surveying is critical to producing an accurate image. Further it must be noted that the exploding reflector model used in this imaging algorithm properly accounts for the primary arrival only, and

multiples are not correctly migrated. Finally, smoothing of the velocity model is required for the RTM procedure to avoid artificial reflections during the wavefield extrapolation. With these caveats, RTM is a valuable tool when producing accurate images in complex and rugged environments is critical.

REFERENCES

[1] Deng, F., and G. A. McMechan, 2007, True-amplitude prestack depth migration: Geophysics, 72, S155–S166.

[2] Fisher, E., G. A. McMehan, A. P. Annan, and S. W. Cosway, 1992, Examples of reverse-time migration of single-channel, ground-penetrating radar profiles: Geophysics, 57, 577–586.

[3] Sanada, Y., and Y. Ashida, 1999, An imaging algorithm for GPR data: Symposium for the Application of Geophysics to Environmental and Engineering Problems 1999, 565-573.

[4] Lehmann, F. and A.G. Green, 2000, Topographic migration of georadar data: Implications for acquisition and processing: Geophysics, 65, 836-848.